Graz University of Technology

Estimation of Reflected UWB Signal Paths

Author: Markus Froehle, 0530038

Date: Graz, February 11, 2011
Rev.: alpha 1.0

Contents

1 Abstract

Within the seminar project an algorithm for detection of Ultra-Wideband (UWB) scatterers proposed by [SKA+08] is implemented and evaluated with indoor measurements. The algorithm tries to resolve single-scatterer extracted from the channel impulse response and assign them to a position in spatial domain. Incorporating the measurements room geometry an extension for finding virtual anchor (VA) nodes is added. Finally, the outcome is discussed and an outlook is provided.

2 Introduction

Indoor localization by using high bandwidth radio signals drew more and more attention in recent research topics. Ultra wide band signals (UWB) are of very interest, because of their large commercially available bandwidth of $3.1 - 10.6$GHz which offers a fine delay resolution and therefore also a fine spatial resolution. For an introduction on UWB see [Mol09]. In [SKA+08] an algorithm for scatterer detection in the spatial domain by using UWB signals was developed. Assuming the known room geometry for localization this algorithm could be expanded in order to find virtual anchor (VA) nodes. [MSW10] defines such VA nodes and how to make use of them for indoor localization.

The report is structured in the following way: First, the project task and measurement scenario is stated. Followed by an explanation of the used algorithm. Then implementation details and the outcome are discussed. Finally, a conclusion and an outlook wraps up this report.

2.1 Project Task

Within the seminar project the functionality of the algorithm developed by [SKA+08] should be verified with data gained from indoor environment. Then a discussion and conclusions for future work should be drawn. The tasks of this project can be described with the following steps

- literature survey
- implementation of the algorithm using MATLAB
- verification of the functionality using data from an indoor measurement, showing additional difficulties
- discussion about the outcome
- conclusions and future outlook.

Furthermore, to support the work around Meissner [MGW10], [MSW10] the algorithm had been extended for finding virtual anchor (VA) nodes.

2.2 Scenario and Measurements

The mode of operation of the algorithm developed by [SKA+08] should be verified with the data gained of a UWB measurement campaign performed at the SPSC laboratory. The measurement scenario is indoor. The floor plan, together with the receiver and transmitter positions, is illustrated in Fig. 2.1. It consists of 381 mobile station (MS) and six base station (BS) positions. The complex channel coefficients between each MS position and all the BS positions were measured. The spacing between two MS positions is 0.1m. A *Rohde and Schwarz ZVA-24* network analyser was used to get the complex channel coefficients for all MS positions. The frequency range is $3.1 - 10.6$GHz with a frequency spacing of 1MHz resulting in 7501 complex channel coefficients for each MS position and for one BS position.

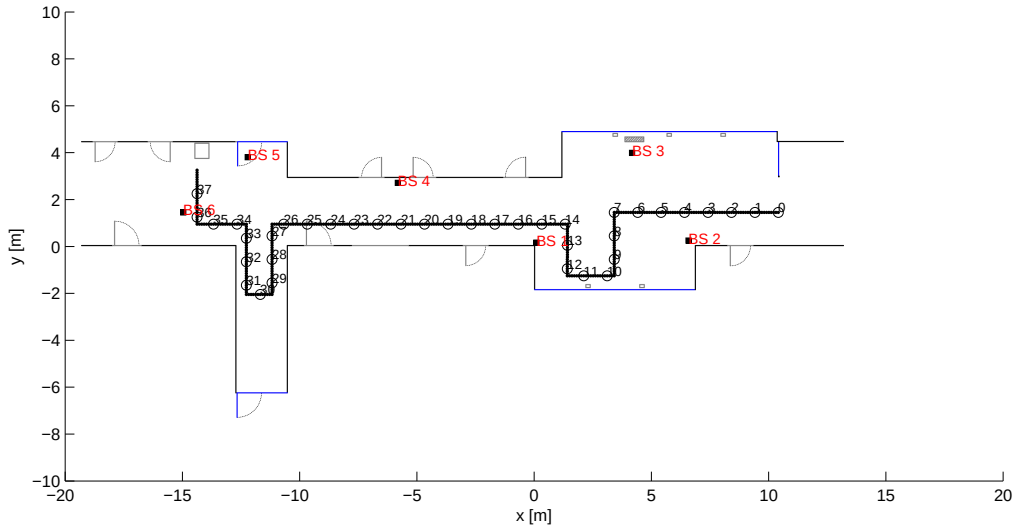

Figure 2.1: Indoor measurement scenario consisting of 381 MS positions and six BS positions.

Fig. 2.2 shows the channel impulse (CIR) response between MS position 70 and BS position three. One can see the first peak at a delay of approximately 10ns, which corresponds to the line-of-sight (LOS). Minor peaks with a delay greater then the LOS correspond to multi-path components (MPCs).

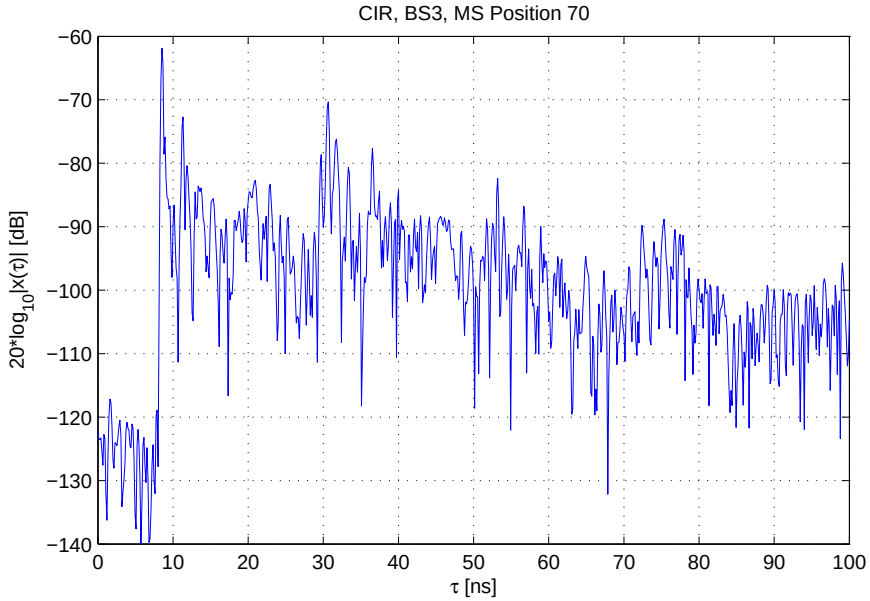

Figure 2.2: Channel impulse response between MS position 70 and BS position three. The highest peak corresponds to the line-of-sight (LOS) path. Minor peaks with a delay greater than the LOS are multi-path components.

A plot containing the CIRs of all MS positions is illustrated in Fig. 2.3. The amplitude of the single CIRs is encoded in colour. In the figure one can see the LOS having the highest peak value. Also there is no peak before the LOS. The higher delay τ starting from MS position 70 to 140 fits to the spatial movement direction of the consecutive MS positions. Between MS position of approximately 265 to 320 there is clearly no LOS component. This fits with the measurement scenario. Also the amplitude of the LOS path is decreasing starting from MS position 200.
Path of peaks over the MS positions with a delay greater than the LOS correspond to MPCs.

The algorithm described below tries to identify such paths and associate them to specific points in the spatial domain.

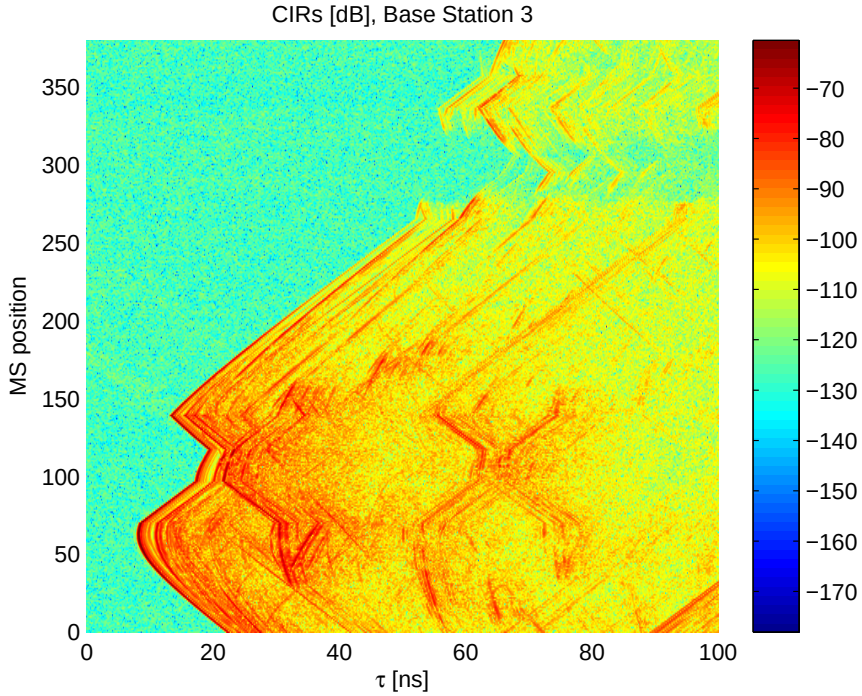

Figure 2.3: Channel impulse responses (CIRs) from MS position one to 381 for BS three. The amplitude of the CIR is encoded in colour. The path with the highest amplitude among the MS positions corresponds to the line-of-sight (LOS). Also there is clearly no peak in the CIRs before the LOS. A path with high amplitude and a delay τ higher than the LOS can be associated to a scatterer point in spatial domain.

2.3 Scatterer Points (SP) and Virtual Anchor (VA) Nodes

Especially for indoor environments not only the LOS has to be considered. A wave travelling from the transmitter is reflected one or more times at several obstacles, e.g. walls, before arriving at the receiver side. For single-scattering processes the point in space where the wave is reflected is called scatterer point (SP).
Taking the floor plan into account the multipath components (MPC) could be mapped to a set of virtual anchor (VA) nodes. VA nodes are mirror images of the anchor with respect to the room walls, or other reflecting surfaces [MSW10]. Herein only first order MPCs are considered. Fig. 2.4 illustrates the two different delays for estimating SP and VA points.

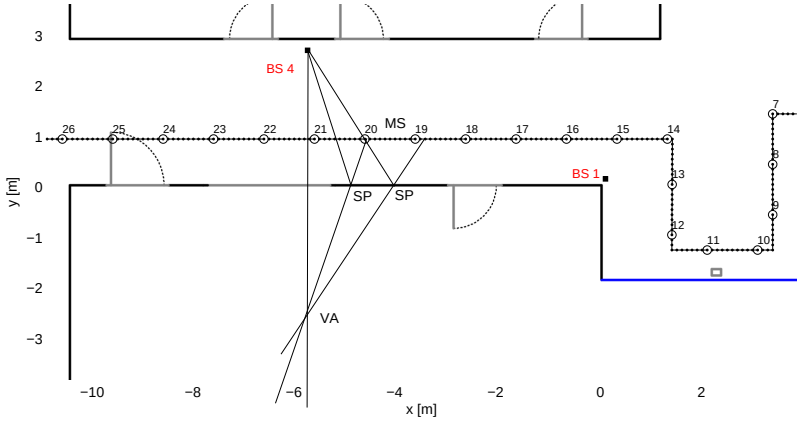

Figure 2.4: Part of the floor plan showing scatter (SP) and virtual anchor (VA) points. A single-scattering wave travels from the transmitter (MS), reflects at the wall (SP) and arrives at the receiver (BS 4). Extending the way between the different MS positions and their scatter point (SP) with a line one can see that they all penetrate through the same imaginary point called the virtual anchor (VA). This point acts as a virtual source representing the wave from these transmitter positions [MSW10].

3 Algorithm for MPC-Extraction

In the following section the assumed signal and channel model together with the algorithm by [SKA+08] will be shortly sketched.

3.1 Signal and Channel Model

A simplified model for the UWB channel impulse response can be written by the summation of closely-spaced scaled impulses

$$x(\tau) = \sum_{k=1}^{L} \alpha_k \delta(\tau - \tau_k) \tag{3.1}$$

where L is the number of MPCs, α_k the corresponding scaling factor and $\delta(\tau)$ the Dirac-delta impulse. The delay τ_k can be described in the spatial domain by the time the wave travels from transmitter (TX), bouncing at the scatterer point (SP) and arriving at the receiver (RX). Neglecting any dialectic media the wave travels with speed of light $c \approx 3 \cdot 10^8 m/s$ corresponding in a delay

$$\tau_{k_{\mathrm{SP}}} = \frac{d(\mathrm{TX}, \mathrm{SP}) + d(\mathrm{SP}, \mathrm{RX})}{c} \tag{3.2}$$

with the geometric distance $d(\mathrm{TX}, \mathrm{SP})$ between the two points TX and SP and $d(SP, RX)$ the distance between SP and RX respectively.
Assuming the wave was emitted from a virtual transmitter, the VA node, the delay is defined by

$$\tau_{k_{\mathrm{VA}}} = \frac{d(\mathrm{VA}, \mathrm{RX})}{c} \tag{3.3}$$

with the geometric distance $d(\mathrm{VA}, \mathrm{RX})$ between the points VA and RX.
Depending on the requirements of the applications whether $\tau_{k_{\mathrm{SP}}}$ or $\tau_{k_{\mathrm{VA}}}$ is used for τ_k. If the algorithm should search for scatterer points the first definition is used. On the other hand, if virtual anchor nodes are of interest the latter one is used. Also a combination of both is possible which will be shown later.
The algorithm by [SKA+08] assumes that the measurement data is based on frequency domain measurements. Each frequency point is defined by a complex channel coefficient. To obtain the channel impulse response $x_r(\tau)$ for the r-th MS position the inverse Fourier transformation has to be computed like

$$x_r(\tau) = \mathbf{p}(\tau)^{\mathrm{T}} \mathbf{h}_r \tag{3.4}$$

with the constant vector

$$\mathbf{p}(\tau) = [e^{j2\pi f_{\min}\tau} \cdots e^{j2\pi(f_{\min}+(N_F-1)\Delta f)\tau}]^{\mathrm{T}} \tag{3.5}$$

for all MS positions and the complex channel coefficients

$$\mathbf{h}_r = [h_{r,0} \cdots h_{r,N_F-1}] \tag{3.6}$$

where $f_{\min}$ denotes the minimum frequency, N_F the number of frequency points, Δf the frequency spacing and τ the continuous delay. The vector $\mathbf{h}_r$ contains the channel coefficients from frequency $f_{\min}$ to $f_{\max}$.

3.2 Method Description

Based on the frequency domain measurements the algorithm detects scatterer points in three computation steps

- step I - High Resolution Peak Search
- step II - Weighing All Candidate Scatterer
- step III - Detection and Cancellation of the Strongest Scatterer.

Fig. 3.1 illustrates the flowchart with the different steps.

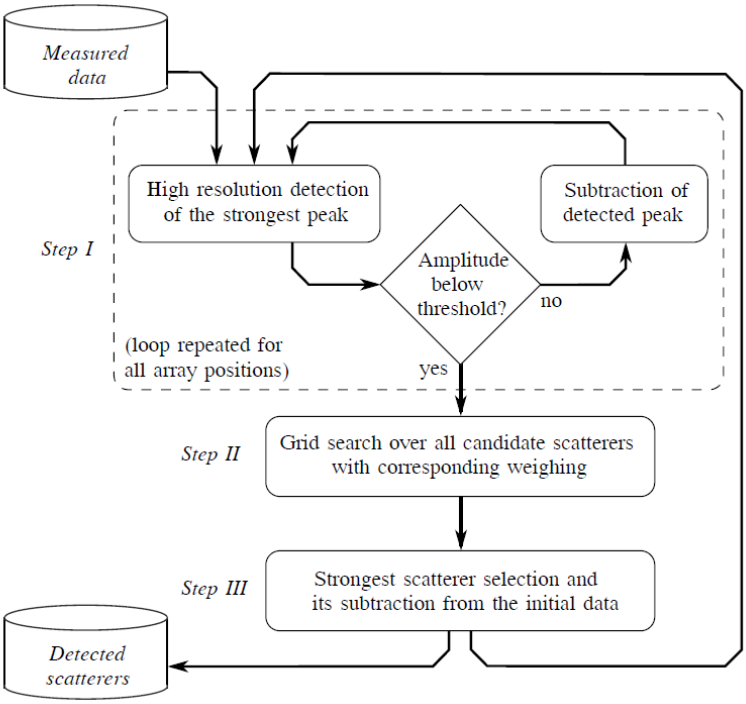

Figure 3.1: Flowchart of the algorithm for scatterer detection by [SKA+08]. Step I: All peaks in all channel impulse responses above the threshold are estimated. Step II: 2-dimensional grid search where every point is assumed to be a candidate scatterer and weighed accordingly. Step III: Subtraction of the strongest scatterer from the channel

The frequency domain measurements consist of a set of complex channel coefficients. Such measurements are obtained with the help of e.g. a Vector Network Analyser. For each mobile station (MS) position a measurement is made. The measured data can be collected in a matrix

$$\mathbf{H} = [\mathbf{h}_1\, \mathbf{h}_2 \cdots \mathbf{h}_{N_R}] \tag{3.7}$$

of the size $(N_F \times N_R)$, where N_F is the number of frequency points and N_R the number of MS positions.

3.2.1 Step I - High Resolution Peak Search

For each MS position r the exact delays and amplitudes of the most significant peaks are estimated in the impulse response $x_r(\tau)$. This is done by an search and subtract approach. First the inverse Fourier transformation of the complex channel coefficients $\mathbf{h}_r$ is computed with the help of Eq. (3.4). Then the delay and amplitude of the highest peak is estimated by

$$\hat{\tau}_{r,l} = \arg\max_{\tau} |x(\tau)| \tag{3.8}$$

$$\hat{\alpha}_{r,l} = x(\hat{\tau}_{r,l}) \qquad \text{with} \qquad \hat{\alpha}_{r,l} > \mu \tag{3.9}$$

where μ is the threshold parameter, $\hat{\tau}_{r,l}$ is the delay and $\hat{\alpha}_{r,l}$ the amplitude corresponding to the l-th highest peak.
Then, the contribution of the l-th peak is subtracted in the frequency domain in the form of

$$\mathbf{h}_{r,l} = \begin{cases} \mathbf{h}_r, & ,l = 1 \\ \mathbf{h}_{r,l-1} - \hat{\alpha}_{r,l-1}\, \mathbf{p}^*(\hat{\tau}_{r,l-1}) & ,l > 1. \end{cases} \tag{3.10}$$

Here, $\mathbf{h}_r$ are the original complex channel coefficients, $\mathbf{h}_{r,l-1}$ the channel coefficients in the previous iteration, $\mathbf{p}^*(\hat{\tau}_{r,l-1})$ the conjugate of Eq. (3.5) at the delay position $\hat{\tau}_{r,l-1}$.
These steps are repeated until all peaks above the threshold parameter μ are determined.

3.2.2 Step II - Weighting All Candidate Scatterer

In this step an identification of the possible geographical scatterer location is done. The geographical search uses a two dimensional grid, where every point k on the grid is assumed to be a candidate scatterer and has a delay time τ_k defined by Eq. 3.2 or 3.3 respectively. Now a comparison is made between τ_k and the delays $\hat{\tau}_{r,l}$ obtained in the previous step for every MS position r. If there is a peak within one delay resolution the peak amplitude is saved in a vector

$$\mathbf{a}_k = [\alpha_{1,k} \cdots \alpha_{N_R,k}] \tag{3.11}$$

for the k-th geographical position. The delay resolution d_{res} is defined by the bandwidth of the used UWB signal for the measurements

$$d_{\text{res}} = \frac{c}{f_{\max} - f_{\min}} \tag{3.12}$$

with $c = 3 \cdot 10^8$m/s the speed of light, $f_{\max}$ the maximum frequency and $f_{\min}$ the minimum frequency respectively.
A tracking of scatterers along the MS positions is done by applying an average sliding window (ASW) over the vector $\mathbf{a}_k$ with

$$\mathbf{w}_k[r] = \frac{1}{N_W} \sum_{n=-N_W/2}^{N_W/2-1} \alpha_{n+r,k} \tag{3.13}$$

where N_W denotes the window size. The first time $\mathbf{w}_k[r]$ exceeds the threshold μ is called the scatterers *birth* location. The scatterers *death* location is reached when it drops below the threshold μ. The scatterer's strength s_k, for position k, is defined by the summation of entries of the vector $\mathbf{a}_k$ which lie within the scatterers *birth* and *death* location.

3.2.3 Step III - Detection and Cancellation of the Strongest Scatterer

The strongest scatterer is first detected

$$s_{k,\max} = \max_k(s_k), \tag{3.14}$$

and then deleted from the channel

$$\mathbf{h}_{r,\text{new}} = \mathbf{h}_r - \hat{\alpha}_{r,l}\, \mathbf{p}^*(\hat{\tau}_{r,l}). \tag{3.15}$$

Here, $\mathbf{h}_r$ denotes the complex channel coefficients for the r-th MS position, $\hat{\alpha}_{r,l}$ the complex amplitude of the peak responsible for the scatterer, the vector $\mathbf{p}^*(\hat{\tau}_{r,l})$ is the conjugate of Eq. (3.5) with the delay of the corresponding peak and $\mathbf{h}_{r,\text{new}}$ the new coefficients.

The three steps are repeated until a satisfying number of scatterer points have been found or no more scatterer points are detected.

3.3 Extension for Finding Virtual Anchor Nodes

The algorithm could be extended for finding VA nodes. Instead of using Eq. (3.2) for estimating the delay τ_k Eq. (3.3) is used. Then VA nodes will be identified and deleted from the channel.

3.4 Extension for Finding both Virtual Anchor Nodes and Scatterer Points

If in every iteration of the algorithm the point with a higher strength, either a scatterer point or a VA node, should be deleted from the channel a search with both delays defined in Eq. (3.2) and Eq. (3.3) has to be performed. This is done by first estimating the strength in step II with $\tau_k = \tau_{k_{\text{SP}}}$ for scatterer points and then with $\tau_k = \tau_{k_{\text{VA}}}$ for VA nodes. The point with higher strength will then be chosen according to

$$s_k = \max(s_{k,\text{scatterer,max}}, s_{k,\text{VA,max}}). \tag{3.16}$$

Here, s_k is the maximum strength of the strongest scatterer $s_{k,\text{scatterer,max}}$ and the strength of the strongest VA node $s_{k,\text{VA,max}}$. The advantage of this method is that due to the same weight estimation always the strongest one will be detected and removed from the channel.

4 Simulation Results

In this section properties and problems of the single steps of the algorithm are discussed. The outcome of the algorithm is stated at the end of this section.

4.1 Simulation Constraints

To limit the modes of freedom and computing complexity only BS four in connection with MS positions one to 200 is considered in detail for the following discussion. The frequency range is restricted form 6 to 8GHz. This results in a worse spatial resolution of

$$d_{\text{spatial}} = c \cdot \tau_{\text{res}} = c \cdot \frac{1}{f_{\max} - f_{\min}} \approx \frac{3 \cdot 10^8}{2 \cdot 10^9} = 15\text{cm} \tag{4.1}$$

where τ_{res} is the delay resolution. $f_{\max}$ and $f_{\min}$ are the maximum and minimum frequency and c the speed of light. In contrast to this using the full UWB band-width from 3.1GHz to 10.6GHz result in a spatial resolution of $d_{\text{spatial}} \approx 4\text{cm}$.
The time delay step $\Delta\tau$ of the high resolution peak search in step I is set four times smaller than the delay resolution by

$$\Delta\tau = \frac{\tau_{\text{res}}}{4}. \tag{4.2}$$

The spatial search step d_{res} of the grid search in step II is set two times smaller than the systems spatial resolution by

$$d_{\text{res}} = \frac{d_{\text{spatial}}}{2} \approx 7.5\text{cm}. \tag{4.3}$$

If not stated differently the simulations were performed searching for both Virtual Anchor nodes and Scatterer Points. In the following discussion both scatterer (SP) points and virtual anchor (VA) nodes are referred to scatterer.

4.2 Step I - High Resolution Peak Search

The importance of a high resolution peak search is illustrated in Fig. 4.1. Considering only the points of the inverse discrete Fourier transformation (IDFT) would not be enough, because the IDFT delivers samples of the channel impulse response at equidistant points in time. Therefore, it is not guaranteed that a resulting sample hits a lobe peak value. To omit this problem the time delay step $\Delta\tau$ has to be small enough in order to determine a lobes peak value.

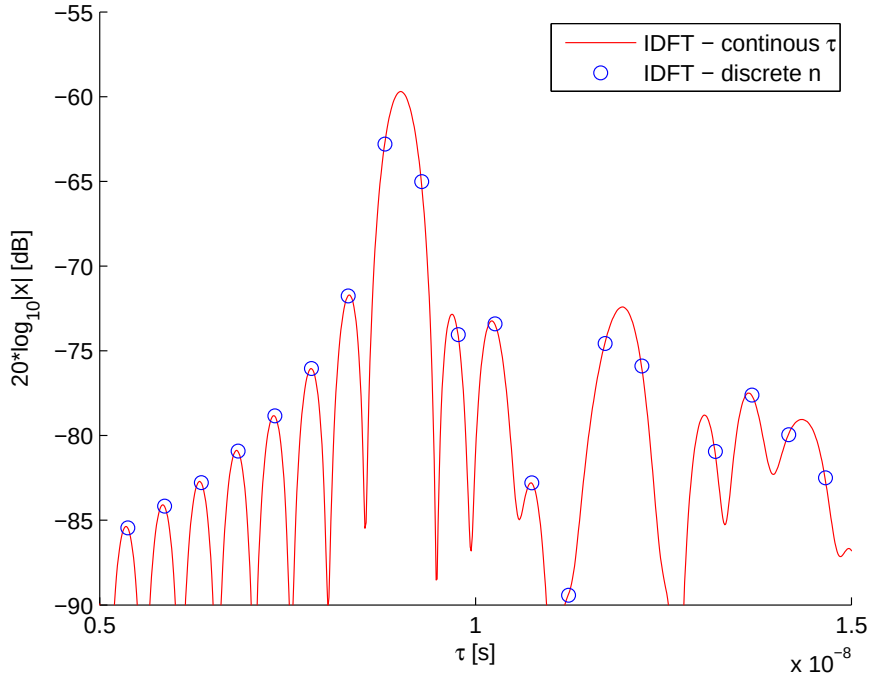

Figure 4.1: Extract of CIR between sender and transmitter. The high resolution peak search is necessary, in order to estimate the exact delay of a lobe peak. Considering only the points of an IDFT is not sufficient. The points of an IDFT not always hit a lobe at its peak.

Once, the maximum peak of the CIR is found it is subtracted from the channel. To do so the subtraction is performed in the frequency domain with the help of Eq. (3.10).
Because of the band-limitation of the input signal (defined by the frequencies $f_{\min}$ and $f_{\max}$) the peak corresponds to a *sinc*-function in time domain. Therefore removing the peak from the channel also effects its neighbourhood. Fig. 4.2 illustrates the subtraction of a peak on the channel in time domain.

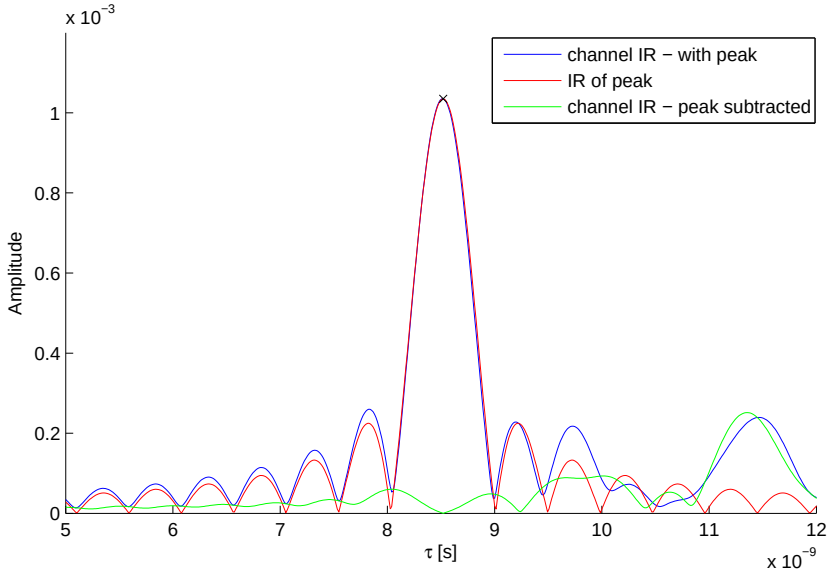

Figure 4.2: The peak is subtracted form the channel. Due to the band-limitation of the input signal the impulse response (IR) of the peak is described by a sinc-function. Removing it from the channel also effects the surrounding lobes.

4.3 Step II - Weighing all Candidate Scatterer

4.3.1 Effects of Threshold Parameter μ

The threshold parameter μ has a number of effects on the behaviour of the algorithm. It defines

- the sensitivity of the algorithm
- the *birth* and *death* location of a scatterer, defined by the average sliding window, which depend on μ
- the scatterer strength.

Depending on the measurement setup and the threshold value μ the number of detected peaks above the threshold varies. Fig. 4.3 contains three plots with all the detected peaks above a threshold $\mu = -80\text{dB}, \mu = -90\text{dB}$ and $\mu = -99\text{dB}$. Only the delay position of a peak is plotted for all MS positions. The number of estimated peaks increases if the threshold μ is decreased. The red path corresponds to the strongest scatterer found in iteration one. The scatterer matches with the LOS path. The black and green path correspond to the strongest scatterer in the next iteration steps.
Step II of the algorithm uses all detected peaks in order to find the strongest scatterer. If the threshold value μ is set too high only a few to none, but strong, scatterer points are found. On the other hand, if μ is too close to the noise floor of the channel IR a lot of peaks are detected, but they might adulterate the outcome resulting in a wrong scatterer detection and deletion from the channel.

4.3.2 Effects of Sliding Window Size N_W

The parameter N_W defines the window size of the average sliding window for computing the k-th scatterer weight $w_k[r]$ at the r-th MS position. A large window size N_W results in a slow change of $w_k[r]$ from the r-th to the $(r+1)$-th MS position, whereas a small window size results in a more agile scatterer weight change.
The scatterer *birth* location is defined when the scatterer weight $w_k[r]$ the first time exceeds the threshold μ. The *death* location is where the weight falls below the threshold μ. An example for a bad and good choice of the window size N_W is illustrated in Fig. 4.4. In the upper plot the window size is too small. The scatterer weight $w_k[r]$ fluctuates too much around the threshold μ and results in a short scatterer lifetime. The scatter *death* is reached shortly after its *birth*. The window size in the lower plot is chosen appropriately. The scatterer lives until a clear drop of the signal amplitude below the threshold appears.
The window size N_W therefore defines how many iterations are needed in order to remove the a scatterer from the channel. If the life-time of a scatterer is estimated too short, caused by an in-proper parameter setting, more iterations were needed to delete the whole scatterer. It is obvious that the scatterer positions found in each iteration are geographically closely spaced together, because the delay of all the peaks in the plot correspond to the delay of the k-th scatter point and are within one delay resolution $\Delta\tau$. In the lower plot a lot of peaks of the channel IRs fall between the scatterer *birth* and *death* and therefore many peaks are deleted from the channel in one iteration.

4.4 Step III - Detection and Cancellation of the Strongest Scatterer

Once the strongest scatterer is estimated it is deleted from the channel. Fig. 4.5 shows the effects of the successive scatterer deletion. The upper plot shows the measured channel impulse response (CIR) for the MS positions 1 to 200. The delay τ is set between 0 and $100ns$. The current amplitude of the impulse response for one MS position is encoded in color reaching from

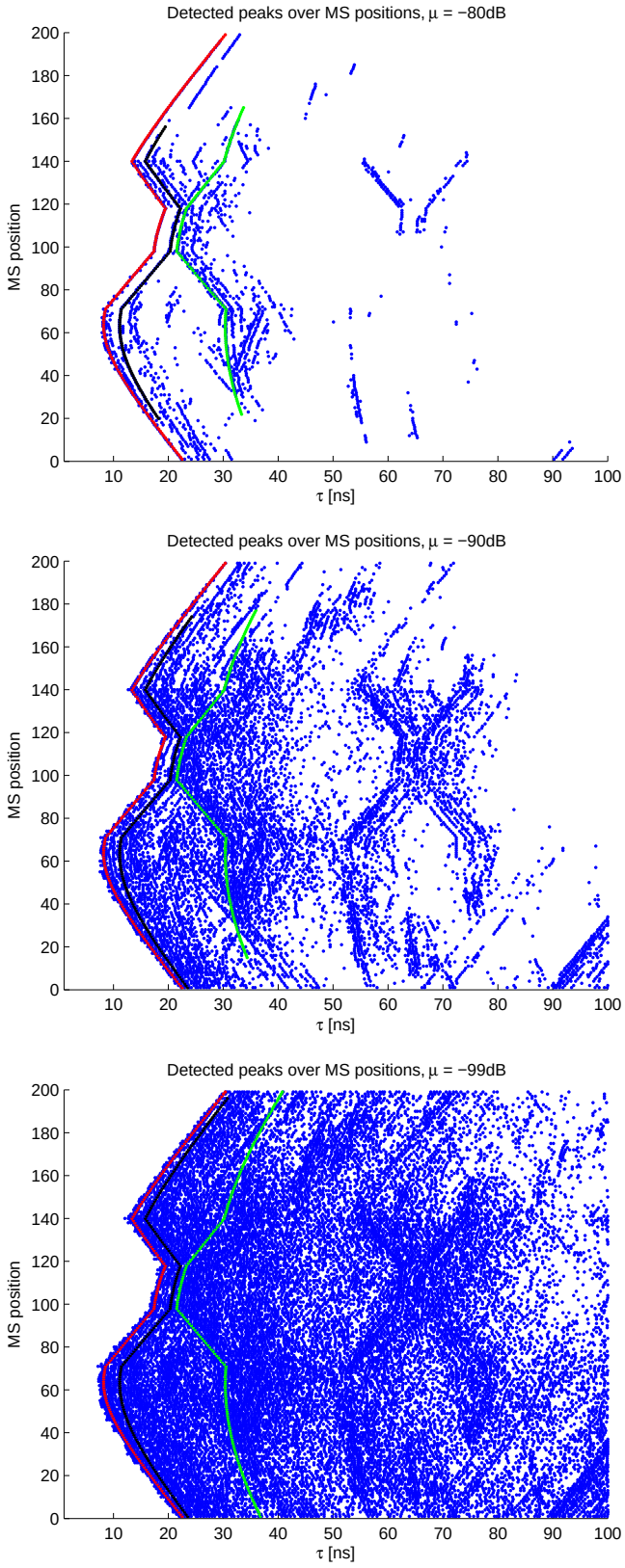

Figure 4.3: Plot of all detected peaks above the threshold value μ for all MS positions (blue points). The red curve shows the highest peak over all MS positions between the scatterer birth and death location which is defined by the average sliding window (ASW). The delay τ complies with the line-of-sight path. The black and green curve correspond to the highest peaks in the next iteration steps.

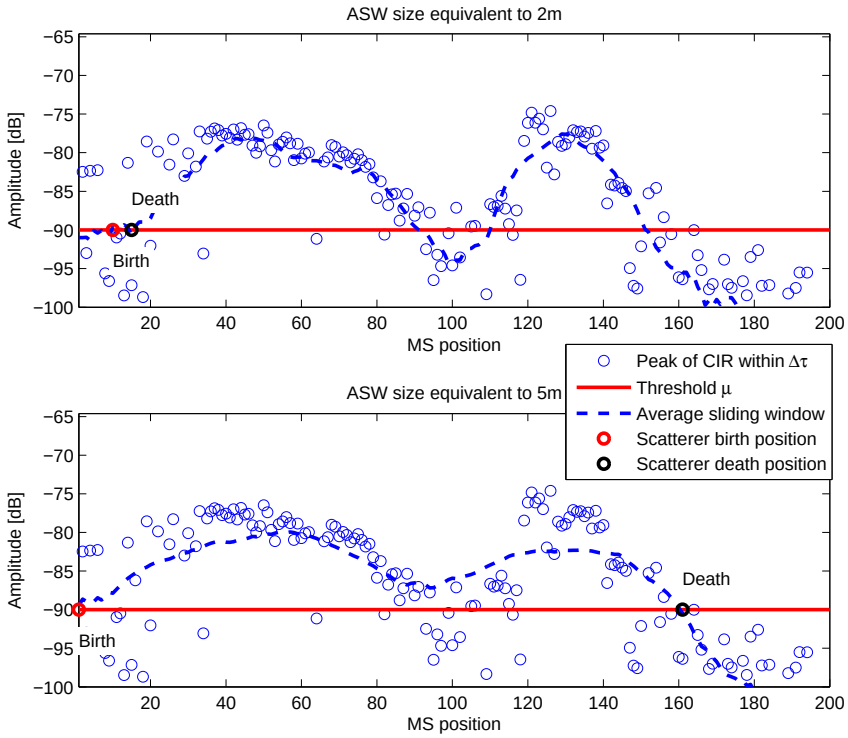

Figure 4.4: Average sliding window of a good scatterer. Upper plot: The window size is too small. Resulting in a fluctuation of the ASW curve around the threshold μ. The scatterer death location is determined too early resulting in a short scatterer life-time. Lower plot: Larger window size equivalent to 5m. The scatterer life-time is chosen appropriately.

approximately −150dB up to −60dB. The line-of-sight component has clearly the strongest amplitude and the lowest delay τ between MS and BS.
The line-of-sight (LOS) *scatterer* is the first one to be selected and removed from the channel by the algorithm. After one iteration the CIRs are shown in the middle plot of the same figure. The predominant amplitudes caused by the LOS *scatterer* are removed now. Within this plot there is a path with peaks of large amplitude between MS position 35 and 130. This path has a longer delay τ than the LOS and corresponds to a different scatterer point. Now this scatterer is estimated by the algorithm and removed in this iteration.
The lower plot verifies this behaviour. In this plot the CIRs are shown after the iteration step two. One can see that the two strongest scatterer of the previous iteration have been removed successfully.

4.5 Outcome - Estimated Scatterer and VA Node Positions

In Fig. 4.6 the scatterer strengths are plotted in spatial domain. The left column shows the entire search space for one iteration. The point with the strongest scatterer strength is marked with a red square. The peaks in the CIRs corresponding to this scatterer point will be removed from the channel. In the next iteration the scatterer is removed and therefore the strength at this point decreased. The right column provides a zoomed version at the position of the highest scatterer strength from the plots on the left-hand side. The expected VA points are marked with a green square and as one can see they are hit very well. Table 4.1 contains the estimated scatterer (SP)/VA nodes. Due to the choice of parameters it is not always possible to cancel the whole scatterer from the channel in one iteration. More iteration steps are needed, but the estimated scatterer positions are closely spaced together in the spatial domain.

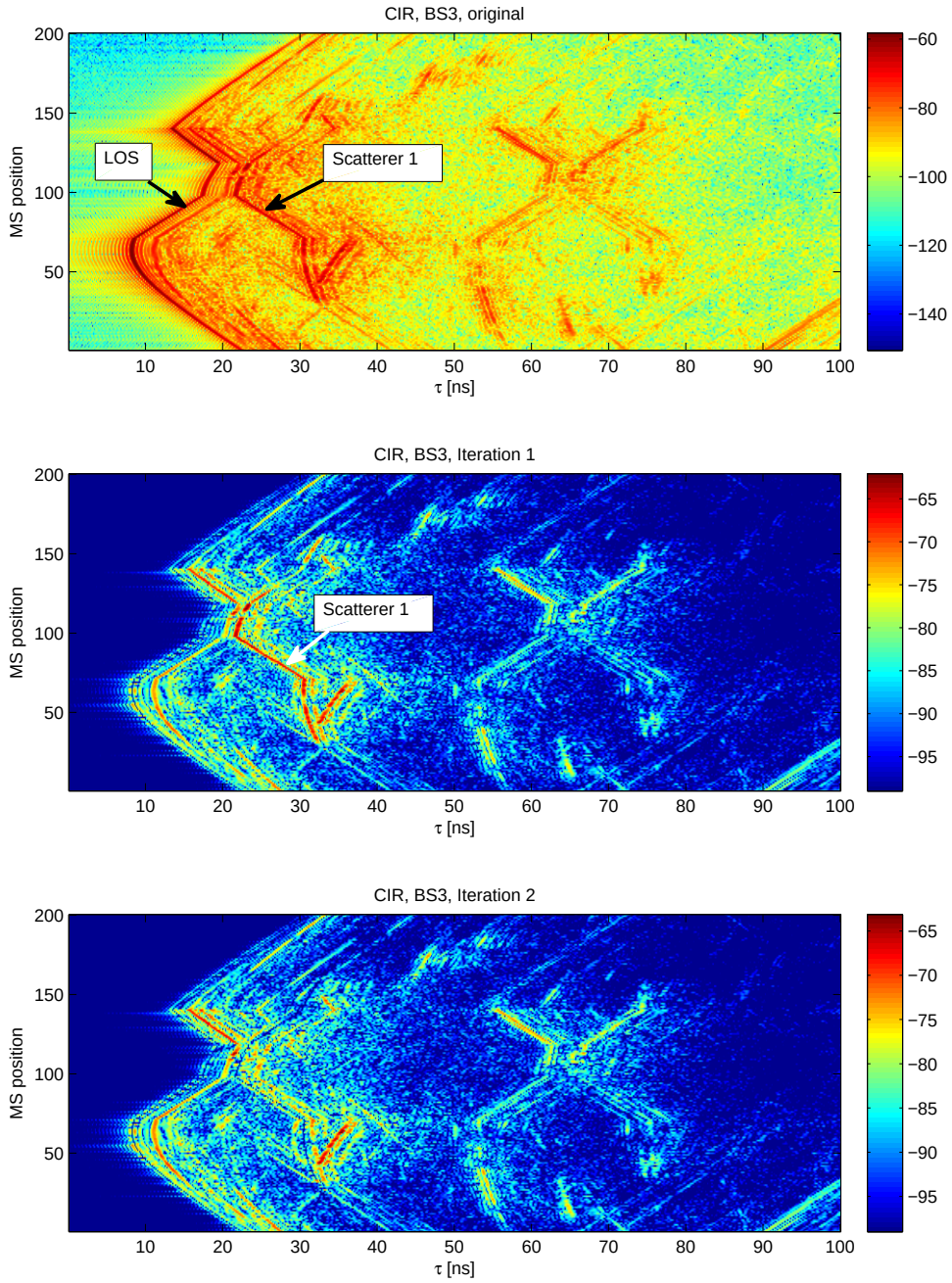

Figure 4.5: Channel impulse response (CIR) between the MS positions 1 to 200 and BS three. The upper most plot shows the measured CIR. The left most strongest path with a high amplitude corresponds to the line-of-sight (LOS). The longer delay τ between MS position 70 and 140 is due to the measurement set-up shown in Fig. 2.1. The artefacts with a shorter delay than the LOS are caused by the rectangular windowing provoked by the band-width limitation from 6 to 8 GHz. The plot in the middle shows the CIR after removing the LOS in iteration one. The LOS path is almost completely removed. The lower plot shows the CIR in iteration two where 'Scatterer 1' has been removed.

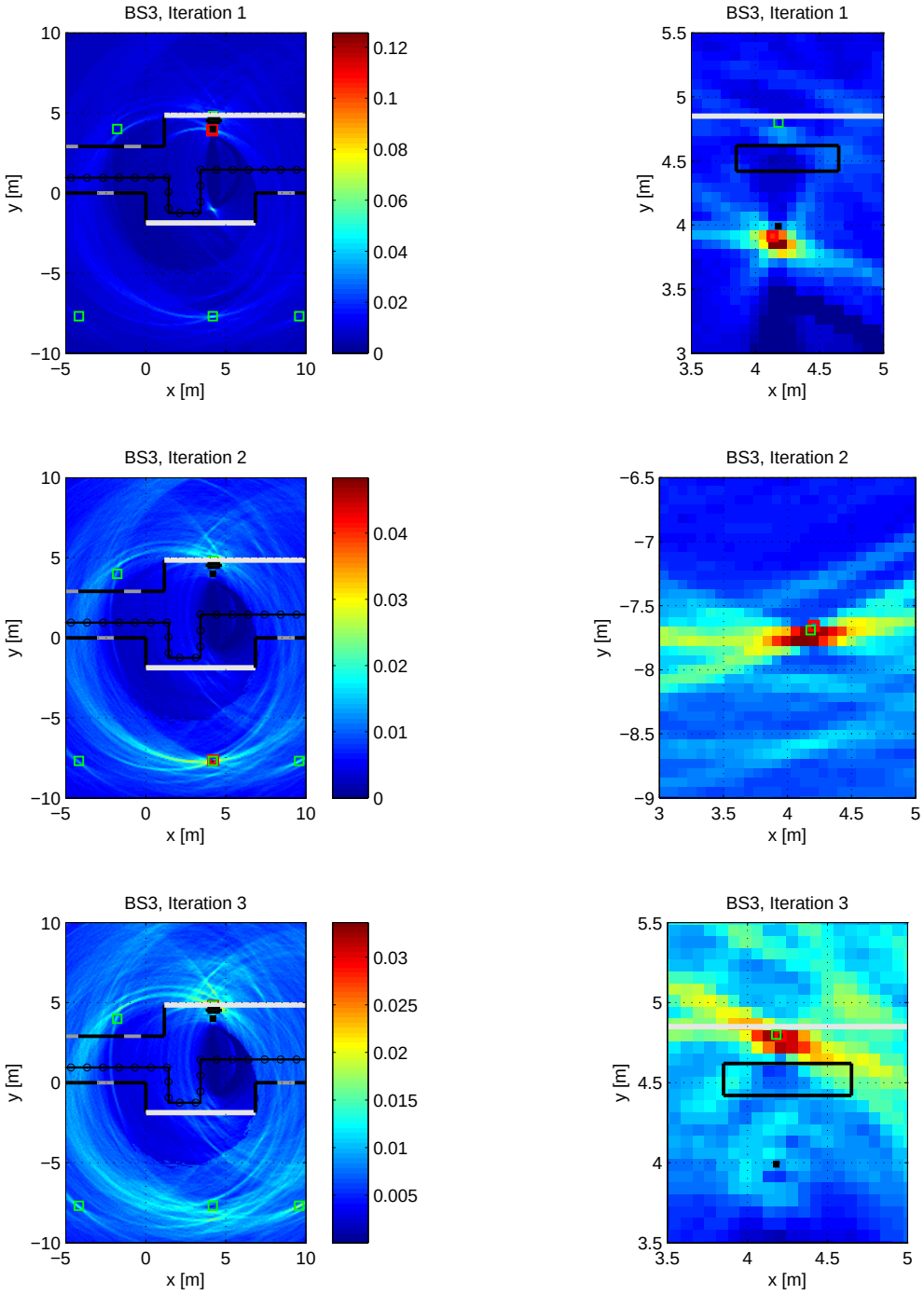

Figure 4.6: Strength of virtual anchor (VA) node for each geographical position. The strongest point is then cancelled from the channel for the next iteration step. Left column: The upper plot shows the strongest VA node found in the first iteration step (marked with a red square). The green squares describe the estimated VA node positions. The MS positions, as well as the floor plan are laid over the VA strengths. Right column: Zoomed view of the computed scatterer position. The expected VA points are hit very well.

Iteration step	Type	X position $[m]$	Y position $[m]$
1	VA	4.13	3.91
2	VA	4.21	-7.66
3	VA	4.13	-7.73
4	VA	4.21	4.79
5	VA	4.21	5.67
6	VA	9.48	-7.73
7	VA	4.13	-8.54
8	SP	3.47	4.65
9	VA	4.06	-8.02
10	SP	5.74	4.57
11	SP	4.13	3.99
12	VA	-4.00	-7.88
13	VA	4.21	5.01
14	SP	4.21	4.13
15	VA	4.28	6.92

Table 4.1: Geographical location of the estimated scatterer (SP)/VA nodes in each iteration step.

The estimated scatterer and VA nodes are plotted in Fig. 4.7. In the plot there are a few scatterer/VA points close to the location of BS three. The delay which fits to BS three is the delay for the LOS path between BS and MS. Also the peak in the CIR which corresponds to the LOS has the highest amplitude for all MS positions. To remove this strong 'scatterer' completely from the channel more than one iteration steps are needed resulting in scatterer/VA points close to the *real* one.

4.6 Comparison of Using Different Frequency Ranges

Performing the simulation with the whole UWB frequency range from $3.1 - 10.6$GHz is computationally demanding. The advantage of the high band-width is the increase of the spatial resolution.
To narrow down the computation effort the peak search in step I of the algorithm has been reduced. In every iteration only the ten most dominant peaks were used for estimation of the scatterer. Fig 4.8 contains the scatterer strength in the spatial domain. One can see the improved spatial resolution compared with Fig. 4.6. The expected and estimated scatterer positions are almost equal.

4.7 Clustering the Estimated Scatterers

In order to estimate the exact position of a scatterer it is well established to cluster scatterer locations [SKA+10]. Clustering of estimated scatterers is not addressed here. For the sake of completeness in [SKA+08] and [SKA+10] they used a modified version of K-means clustering. The K-means algorithm minimizes the euclidean distance between data points to find its centre. By using a power-weighed distance metric scatterer with a high weight have a greater impact on estimating the scatterers centre.

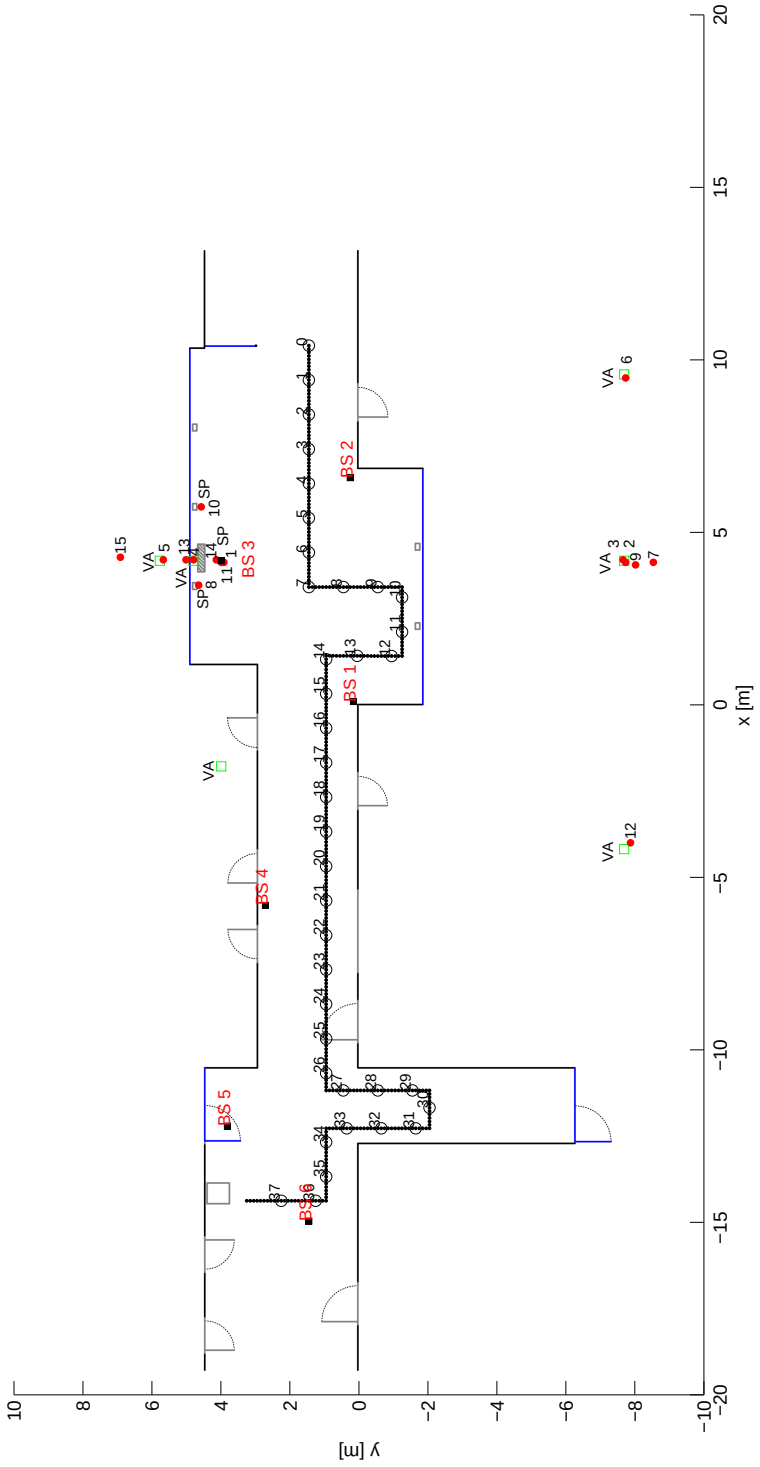

Figure 4.7: Estimated VA nodes and scatterer locations (SP). Evaluated for 15 iterations. In the plot the floor plan together with the position of the base stations (BS) and mobile stations (MS) are illustrated. The expected virtual anchor (VA) nodes are marked with a green square. The estimated VA and SP locations are marked with a red dot. Additionally the SP points are labelled. BS three corresponding to the line-of-sight path, the strongest VA nodes and scatterer locations are found very well.

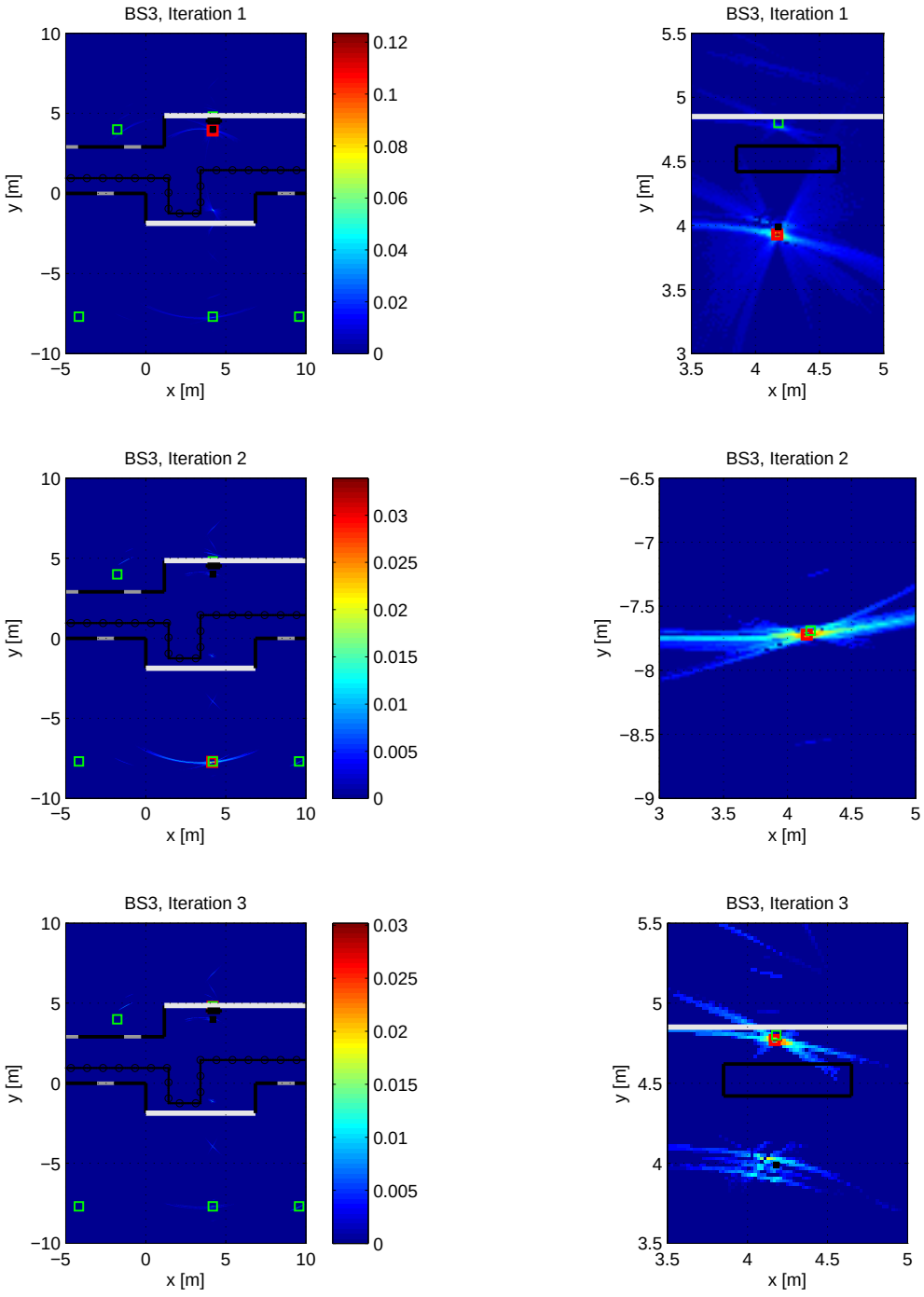

Figure 4.8: The same plot as in Fig. 4.6, but here the simulation was performed using the whole UWB frequency range of $3.1 - 10.6\,GHz$*. Also only the ten most dominant peaks in step I were used for estimation of the scatterer resulting in a sparsity of strength in the plots. The spatial resolution has improved compared with using the frequency range of* $6 - 8\,GHz$*.*

4.8 Problems

4.8.1 Ambiguity of Scatterer Points

In order to estimate a scatterer position in spatial domain the algorithm compares its delay τ with the delay of the peaks exceeding the threshold μ in all CIRs. This can lead to ambiguous scatterer points in space if the MS positions trajectory is a straight line. In the upper left plot of Fig. 4.6 there is a point with high amplitude exactly at the horizontally down flipped position of BS three having the coordinates $[4.2, -1.0]^{\mathrm{T}}$. This scatterer point belongs to the scatterer at the location of BS three. Once the scatterer at BS three is removed from the channel the ambiguous scatterer is also removed. This can be seen in the middle plot of the first column in the figure. There the ambiguous scatterer disappeared completely.
Ambiguous scatterer points are a real problem in measurement set-ups where the MS positions trajectory is a straight line. The algorithm has no knowledge if the strongest scatterer corresponds to a real or to an ambiguous one. Then the estimated scatterer position might be wrong.

4.8.2 Computing Complexity

The high resolution peak search in step II and a large search space for the grid search in step III lead to time consuming computations in each iteration of the algorithm. A reduction of computing effort in step II can be obtained by

- decreasing the resolution $\Delta\tau$ of the peak search
- reducing the band-width of the signal
- reducing the maximum delay of the channel IR
- increasing the threshold parameter μ.

And for step III

- reducing the search space
- decreasing the resolution d_{res} of the grid search.

5 Conclusion and Outlook

5.1 Conclusion

[SKA+08] demonstrated a simple method for scatterer detection using UWB signals. It had been showed that the algorithm could be extended for finding virtual anchor (VA) nodes. The evaluation of the algorithm shows that the expected scatterer points and VA nodes are found very well. Increasing the band-width, which increases the systems spatial resolution, results in a more exact estimate of the real scatterer location. Also the deviation between the estimated and expected scatterer location enlarges for successive estimates. The measurement data used for evaluation was gained indoor. Reflections on the ground and ceiling had heirin been omitted completely. Also only simple reflections are evaluated by this algorithm. This might not be a valid assumption. In [SKA+08] the measurement scenario was outdoor expecting almost only LOS and single bounce paths.

5.2 Outlook

An optimization of the high resolution peak search would significantly increase the execution speed. Incorporating the floor plan allows to limit the search space of the grid search. For an indoor measurement scenario reflections at the floor and ceiling should also be considered. This results in a 3-dimensional scatterer localization. Making use of higher order MPCs would further increase the accuracy of the algorithm. The definition of a scatterers *birth* and *death* location gives additional information about its confidence which could as well be incorporated. Furthermore, an online method of this algorithm would allow real-time tracking and detection of scatterer.

Bibliography

[MGW10] P. Meissner, T. Gigl, and K. Witrisal. UWB sequential Monte Carlo positioning using virtual anchors. In *Indoor Positioning and Indoor Navigation (IPIN), 2010 International Conference on*, pages 1 –10, 2010.

[Mol09] A.F. Molisch. Ultra-Wide-Band Propagation Channels. *Proceedings of the IEEE*, 97(2):353 –371, 2009.

[MSW10] Paul Meissner, Christoph Steiner, and Klaus Witrisal. UWB positioning with virtual anchors and floor plan information. In *Positioning Navigation and Communication (WPNC), 2010 7th Workshop on*, pages 150 –156, 2010.

[SKA+08] T. Santos, J. Karedal, P. Almers, F. Tufvesson, and A.F. Molisch. Scatterer Detection by Successive Cancellation for UWB - Method and Experimental Verification. In *Vehicular Technology Conference, 2008. VTC Spring 2008. IEEE*, pages 445 –449, May 2008.

[SKA+10] T. Santos, J. Karedal, P. Almers, F. Tufvesson, and A. Molisch. Modeling the ultra-wideband outdoor channel: Measurements and parameter extraction method. *Wireless Communications, IEEE Transactions on*, 9(1):282 –290, 2010.